Oncogene (2014) **33,** 2329–2340

www.nature.com/onc

ORIGINAL ARTICLE

H-Ras-driven tumoral maintenance is sustained through caveolin-1-dependent alterations in calcium signaling

A Rimessi, S Marchi, S Patergnani and P Pinton

A growing body of research has highlighted the complex range of tumoral traits acquired during H-Ras-driven transformation and maintenance, which include proliferative signaling, growth suppressor evasion and resistance to cell death. Clear molecular information about these processes is not yet available, but recent evidence has provided solid support for the importance of mitochondria. Here, we show that the induction of oncogenic H-Ras leads to changes in intracellular calcium (Ca^{2+}), evaluate the temporal relationship between oncogene expression and mitochondrial physiology, and demonstrate that Ca^{2+} homeostasis is altered by caveolin-1, a protein that has a key role in tumor maintenance. Our results indicate that tumor-suppressor caveolin-1 is a core component of the Ca^{2+}-dependent apoptotic pathway and participates in the regulation of critical mitochondrial functions during tumor development. The compromised caveolin-1/Ca^{2+} axis contributes to failure in both mitochondrial metabolism and apoptosis, thereby sustaining the neoplastic phenotype. These results illustrate a direct link between Ca^{2+} regulation and mitochondrial biology in cancer.

Oncogene (2014) **33,** 2329–2340; doi:10.1038/onc.2013.192; published online 3 June 2013

Keywords: calcium signaling; caveolin-1; mitochondria; apoptosis; oncogenic H-Ras

INTRODUCTION

The expression of specific oncoproteins, such as Ras, allows the maintenance of tumor survival and proliferation. The Ras oncogene is mutated in 33% of all human cancers, and the highest mutation frequency is observed in cancers with few therapeutic options. Ras proteins are GTPases that are activated by receptor tyrosine kinases and transduce extracellular signals to the nucleus,[1] initiating multiple signaling cascades.[2] One important area of cancer research is represented by 'oncogene addiction' described as the dependency of tumor cells on the activity of a single oncogene.[3] This phenomenon occurs in several mouse models of common cancers[4] where the complete regression is given to massive apoptosis when oncogene expression is shut off.[3] These observations indicate that the continued production of oncogenic Ras is required to sustain the tumor.

Warburg was the first to hypothesize that mitochondrial impairment is a leading cause of cancer and that the prominent feature of cancer metabolism is the reallocation of ATP synthesis from the mitochondria to glycolysis.[5] Despite the observation that tumor cells exhibit high levels of aerobic glycolysis, the role of mitochondria in tumor cell metabolism has been contentious. Several reports have provided mechanistic details and solid support for the importance of mitochondria in driving the process of malignant cell transformation.[6,7] The role of mitochondria in the energy metabolism, redox biology and apoptosis of cancer cells has been reviewed extensively.[8–10] Alterations in mitochondrial function may be partially responsible for pathogenesis of cancer by sustaining tumor induction and maintenance.[11]

All mitochondrial functions discussed above are mutually linked by a common key element: the Ca^{2+} ion, which is the most versatile cellular messenger.[12] Work by our group and others have shown that mitochondria receive Ca^{2+}-mediated inputs upon stimulation by physiological agonists or toxic agents.[13] The precise role of the immense elevation in mitochondrial Ca^{2+} concentration ($[Ca^{2+}]_m$) is not completely clear, although some data indicate that it might be related to the regulation of mitochondrial function,[14] including respiratory activity[15] and mitochondrial reactive oxygen species (ROS) production.[16]

It is common knowledge that extracellular stimuli induce an increase in cytosolic Ca^{2+} concentration ($[Ca^{2+}]_c$) with defined amplitudes and kinetics through diverse mechanisms.[17] An extensive Ca^{2+}-signaling toolkit is used to assemble signaling systems with very different spatial and temporal dynamics. The restriction of Ca^{2+}-entry pathways to specific microdomains favors efficient communication, facilitating dynamic cellular signaling through a perfect niche for clustering receptors, channels, pumps, exchangers and protein scaffolds.[18] The caveolae constitute a strategically plasma membrane (PM) microdomain,[19] a subset of lipid rafts widely expressed and implicated in numerous cellular functions.[20,21] Caveolin-1, an integral membrane protein, is the principal component of caveolae *in vivo*. The protein contains the conserved caveolin-interacting domain that is essential for its binding to many signaling proteins[19] and for transport of cholesterol to PM.[22] Studies have demonstrated that caveolae contain complex sets of Ca^{2+}-signaling molecules,[23–26] suggesting to regulate Ca^{2+} entry.[27] Thus, caveolae and caveolin-1 can provide a platform for the assembly of diverse Ca^{2+}-signaling complexes, which are critical for the spatial and temporal regulation of Ca^{2+} signal in cancer biology.[28]

In the current study, we have used oncogenic H-Ras (H-Ras_{12V}) to investigate the precise time course of H-Ras-induced changes in

Deparment of Morphology, Surgery and Experimental Medicine, Section of General Pathology, Interdisciplinary Center for the Study of Inflammation (ICSI), Laboratory for Technologies of Advanced Therapies (LTTA), University of Ferrara, Ferrara, Italy. Correspondence: Professor P Pinton, Department of Morphology, Surgery and Experimental Medicine, Section of General Pathology, Interdisciplinary Center for the Study of Inflammation (ICSI), Laboratory for Technologies of Advanced Therapies (LTTA), University of Ferrar, Via Borsari, 46, Ferrara 44121, Italy.
E-mail: pnp@unife.it
Received 26 October 2012; revised 8 April 2013; accepted 15 April 2013; published online 3 June 2013

Ca^{2+} signaling relative to changes in mitochondrial physiology. The use of this experimental system enabled us to identify two key players, the Ca^{2+} and caveolin-1, those seem to be essential for the maintenance of the oncogenic phenotype in H-Ras-transformed cells. The compromised caveolin-1/Ca^{2+} axis contributes to alterations in the mitochondrial metabolism and a failure in apoptotic machinery demonstrating a direct link between Ca^{2+} regulation and mitochondrial biology in cancer.

RESULTS

A retroviral vector expressing H-Ras_{12v} was used to transform 3T3NIH fibroblasts, allowing the examination of the effects of mutant Ras on Ca^{2+} signaling and oncogene-induced neoplastic progression and maintenance. Stable clones were isolated and monitored during their development (from the first hour of transduction until 30 days of stable transformation), and a time-series effect analysis was performed.

The induction of H-Ras_{12v} led to a dramatic change in cell morphology after 6 days; parental 3T3NIH cells showed no morphological changes upon transduction with an empty vector (Figure 1aI), whereas oncogene-expressing cells showed a fully transformed phenotype, characterized by a condensed nuclei, increased refractability and spindle-like morphology (Figure 1aI).

In addition, the stable expression of the oncogene led to cellular expansion (Figure 1aII) and the formation of colonies in soft agar, with higher plating efficiency and larger colony sizes than untransformed cells (Figure 1aIII). Indeed, we investigated the putative preferential sublocalization of H-Ras after the acquisition of the neoplastic phenotype through cell fractionation experiments,[29] as reported in Figure 1b. Both in control and transformed cells, H-Ras localizes to the cytosol, mitochondria, endoplasmic reticulum (ER) and the mitochondria-associated membrane (MAM).[30] The localization of the oncogene at the sites of close interaction between the mitochondria and ER could be crucial for the highly efficient transmission of Ca^{2+} from the ER to the mitochondria.[31] In addition, this location may serve as a strategic point to control fundamental processes involved in energy production and cell fate determination by triggering or preventing apoptosis.[10] All subcellular fractions evaluated are critical Ca^{2+} compartments involved in Ca^{2+} signaling transduction.

We then investigated the effect of H-Ras_{12v} expression on intracellular Ca^{2+} homeostasis in 3T3NIH using specific targeted aequorin probes,[32] because we hypothesized that altered Ca^{2+} homeostasis sustained by H-Ras_{12v} might be necessary for tumorigenesis and tumor maintenance. We performed experiments at different time points to establish a correlation between Ca^{2+} modification and neoplastic transformation. We considered four time points: 24 and 36 h after the tumor induction phase, a 'pretransformed' phase (after 7 days of H-Ras_{12v} expression, when morphological alterations are evident) and the 'later transformation' phase (after 30 days of H-Ras_{12v} expression, when neoplastic compensatory mechanisms are established). All conditions considered were compared with the untransformed condition (mock).

To determine whether changes during H-Ras-driven transformation are accompanied by mitochondrial Ca^{2+} perturbations, transformed and untransformed cells were transduced with mitochondrially targeted aequorin. These experiments employed the IP3-agonist bradykinin, which is known to operate through distinct surface membrane receptors to promote ER Ca^{2+} mobilization (Figure 1c). $[Ca^{2+}]_m$ measured at different time points, revealed important changes in Ca^{2+} levels during tumoral progression, as reported in panels Figure 1cII and cIII-IV. After 36 h of oncogenic transformation, a significative increase in the mitochondrial Ca^{2+} uptake was observed, but this increase was completely reversed after 7 days of tumor induction, with a ~40% $[Ca^{2+}]_m$ reduction in transformed cells, compared with control. This reduction was also maintained at 30 days of oncogene expression (Figure 1d and Table 1).

Interestingly, similar effects on the $[Ca^{2+}]_m$ have been observed after the expression of H-Ras_{12v} in PML-null and p53-null mouse embryonic fibroblasts (MEFs) or E1a-overexpressing MEFs, in which the oncogene promoted tumor-like behavior (Figures 1e, f and Table 1).[33,34] The modification of $[Ca^{2+}]_m$ mediated by H-Ras_{12v} is independent by deletion of specific tumor suppressors or by overexpression of specific oncogenes, as suggested by studies performed in different cell types. Indeed, this effect is specific to H-Ras; the overexpression of another oncogene (E1a) in 3T3NIH does not promote an increase in $[Ca^{2+}]_m$ (data not shown).

To better define the effect of H-Ras_{12v} on mitochondria and its role in mitochondrial Ca^{2+} perturbations, we analyzed the changes in mitochondrial physiology. Important parameters related to mitochondrial Ca^{2+} accumulation were considered, such as mitochondrial structure, membrane potential and ROS production. A comparison of the H-Ras-driven mitochondrial dysfunction at 36 h and 30 days of oncogene expression is shown in Figure 2.

The morphological analyses of the mitochondrial and reticular network, shown by mitochondrially targeted green fluorescent protein and the ER-tracker-RED, respectively, are shown in Figure 2a. No significant alterations in the ER morphology were observed, whereas a time-dependent change in the mitochondrial morphology of transformed cells was detected. In the early phase of tumor induction, the mitochondrial network responds by increasing the mitochondrial volume (Figure 2b), the number of organelles (Figure 2c) and the ER–mitochondrial interactions (Figure 2d), as measured by morphometric analyses. As previously shown, modifications in the $[Ca^{2+}]_m$ are followed by specific changes in mitochondrial morphology. As expected during the later phase of transformation, when the mitochondrial Ca^{2+} uptake is drastically reduced, there is no evidence of mitochondrial network perturbations.

We measured the mitochondrial transmembrane potential ($\Delta\Psi$) using tetramethyl-rhodamine-methylester (TMRM) dye. Mitochondria exhibit an increased $\Delta\Psi$ in H-Ras_{12v}-transformed cells compared with control (Figure 2e). Surprisingly, the $\Delta\Psi$ during the later transformation phase was approximately 60% higher than that of control fibroblasts. To determine whether the increased $\Delta\Psi$ observed in the early and later stages of transformation led to an effective increase in $[Ca^{2+}]_m$, we measured the mitochondrial Ca^{2+} affinity in permeabilized cells. Transformed cells were perfused with a solution mimicking the intracellular milieu (intracellular buffer; IB), then permeabilized with 20 μM digitonin and treated with thapsigargin (2 μM), a specific inhibitor of Ca^{2+} pumps in the ER, in order to completely empty the ER Ca^{2+} stores. The perfusion buffer was then changed to IB with an ethylene glycol tetraacetic acid-buffered $[Ca^{2+}]$ of 1 μM, eliciting an increase in $[Ca^{2+}]_m$ (Figure 2f). The $[Ca^{2+}]_m$ increase was larger in H-Ras-driven tumor cells, which demonstrated approximately 50% higher uptake than control cells (Figure 2fIII).

Finally, we stained the cells with the mitochondrial superoxide indicator MitoSox. We found that H-Ras_{12v}-expressing cells exhibited an increase (~35%) in mitochondrial superoxide production at 36 h after induction (Figures 2gI), whereas was even higher in fully transformed cells (Figure 2gII).

Taken together, these data suggest that in the first hours of transformation, the mitochondria of cells expressing H-Ras_{12v} are more responsive to cellular demands. This mitochondrial hyperactivity appears to be mediated by a major change in $\Delta\Psi$ and Ca^{2+} affinity/accumulation, followed by extensive mitogenesis. This adaptive mitochondrial phenotype was partially maintained

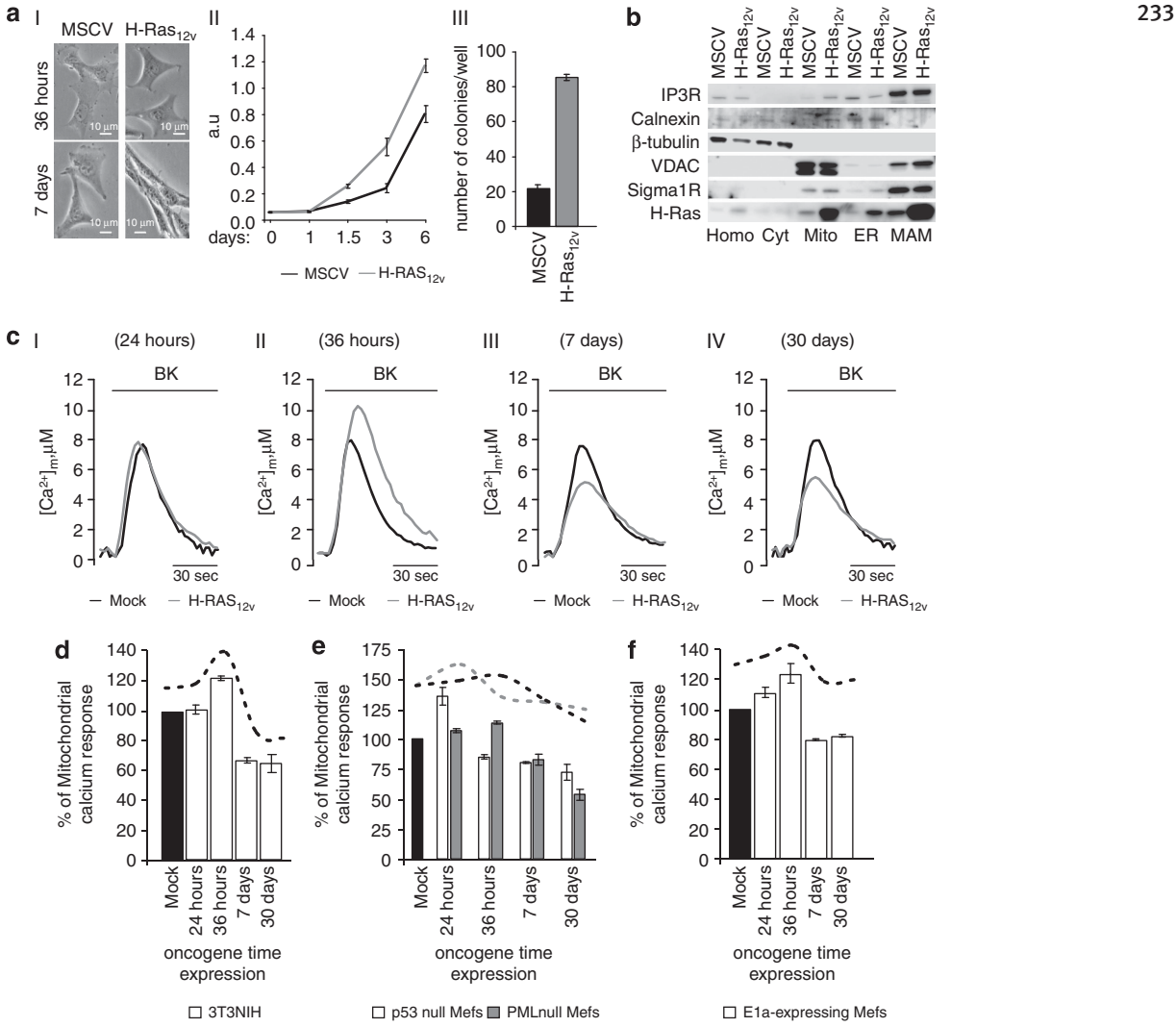

Figure 1. The characterization of the time-dependent effects of H-Ras_{12v} expression on mitochondrial Ca^{2+} homeostasis. (**aI**) Morphological changes induced by oncogenic H-RAS_{12v} in 3T3NIH cells. (**aII**) Growth curve at 1, 1.5, 3 and 6 days of oncogenic H-Ras and empty vector expression in 3T3NIH cells (Murine Stem Cell Virus system; MSCV : T0: 0.031 ± 0.002, T1: 0.036 ± 0.005, T1.5: 0.111 ± 0.012, T3: 0.212 ± 0.035, T6: 0.776 ± 0.064 vs H-Ras_{12v}: T0: 0.035 ± 0.005, T1: 0.039 ± 0.005, T1.5: 0.259 ± 0.015, T3: 0.555 ± 0.065, T6: 1.171 ± 0.053). (**aIII**) Soft agar colony formation assay for fully H-Ras_{12v}-transformed and untransformed cells. Three independent assays were quantified (*n* of MSCV colonies: 21.6 ± 2.4; *n* of H-Ras_{12v} colonies: 85.3 ± 1.8). (**b**) Detailed subcellular localization of Ras in fully transformed cells. The oncoprotein localizes to the cytosol (Cyt) and mitochondria (Mito) in the ER and MAM fractions (Voltage-dependent anion channel (VDAC) and Inositol 1,4,5-trisphosphate receptor (IP3R)). (**c**) Representative mitochondrial Ca^{2+} measurements in mock and H-Ras_{12v}-driven tumoral cells. A mitochondrial-targeted aequorin probe was used to investigate the mitochondrial Ca^{2+} modification introduced during neoplastic progression upon incubation with 1 μM of bradykinin. (**I**) At 24 h of expression: $[Ca^{2+}]_m$ in mock (7.42 ± 0.40 μM) vs H-Ras_{12v} (7.56 ± 0.46 μM); (**II**) at 36 h of expression: $[Ca^{2+}]_m$ in mock cells (8.12 ± 0.75 μM) vs H-Ras_{12v} (10.20 ± 0.89 μM); (**III**) at 7 days of expression: $[Ca^{2+}]_m$ in mock cells (7.49 ± 0.25 μM) vs H-Ras_{12v} (5.03 ± 0.26 μM); (**IV**) at 30 days of expression: $[Ca^{2+}]_m$ in mock cells (8.06 ± 0.31 μM) vs H-Ras_{12v} (5.53 ± 0.45 μM). (**d**) Percent change in the mitochondrial Ca^{2+} response in H-Ras_{12v}-transformed 3T3NIH cells, (**e**) p53/PML-*null* cells and (**f**) E1a-expressing fibroblasts, compared to controls. All data are summarized in Table 1.

Table 1. Percent change in the mitochondrial Ca^{2+} response in H-Ras_{12v}-transformed 3T3NIH cells, p53/PML-*null* cells and E1a-expressing fibroblasts, compared with controls

H-Ras_{12v} trasforming	T *24 h*	T *36 h*	T *7 days*	T *30 days*
3T3NIH	102.8 ± 3.0	124.2 ± 1.8	68.9 ± 3.6	64.8 ± 5.7
p53 *null* MEF	143.0 ± 7.7	89.3 ± 2.0	84.7 ± 0.9	76.2 ± 7.3
PML *null* MEF	106.5 ± ± 1.3	111.8 ± 1.3	82.3 ± 4.2	53.4 ± 4.3
E1a-expressing MEF	111.1 ± 3.4	123.5 ± 6.8	79.0 ± 0.5	81.7 ± 1.0

Abbreviation: MEF, mouse embryonic fibroblast. In the table are summarized the data of Figures 1d–f.

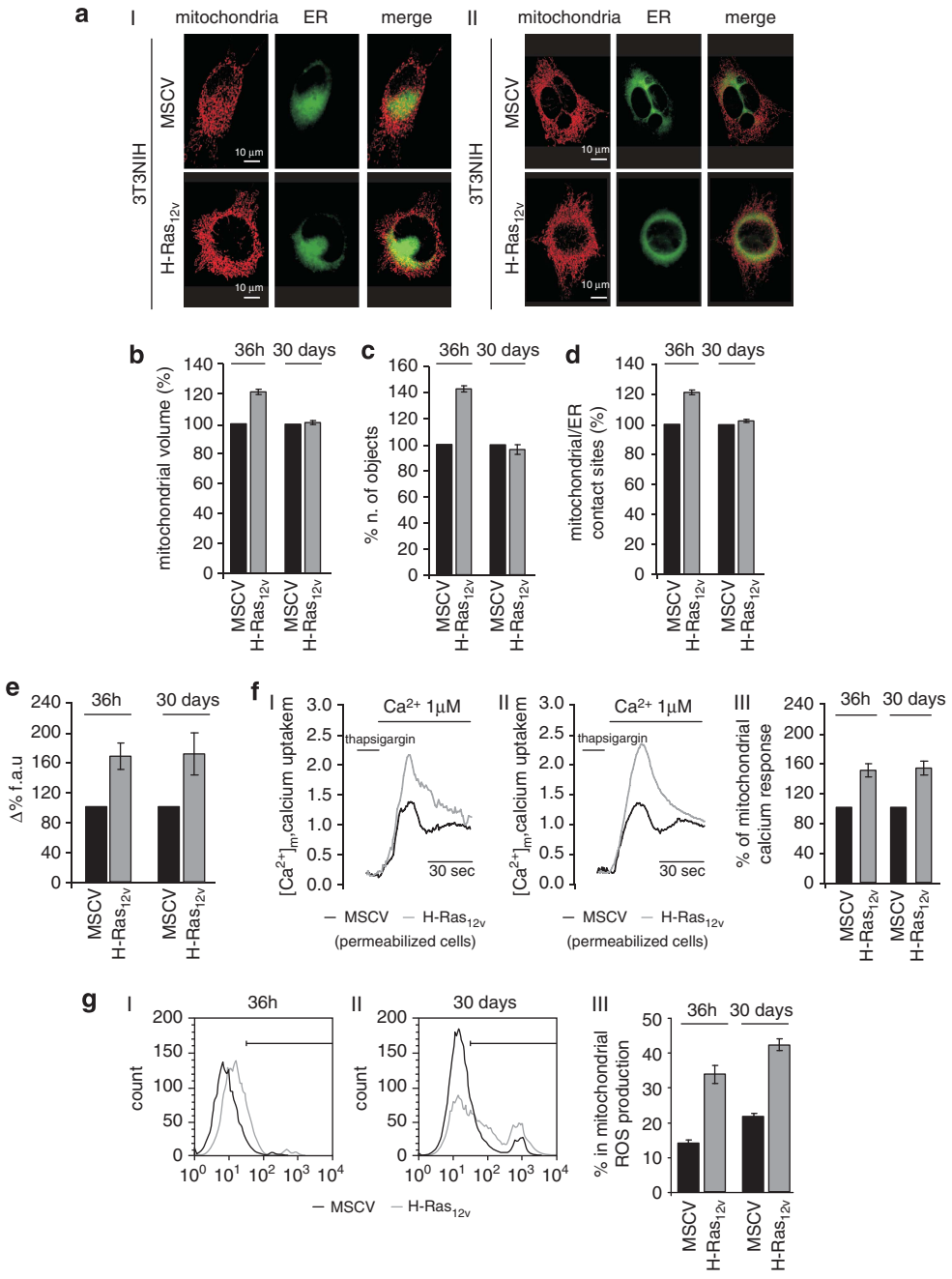

Figure 2. Oncogenic stress induces mitochondrial dysfunction during neoplastic transformation. (**a**) Representative confocal images of the mitochondria and ER in mock and H-Ras_{12v}-transformed 3T3NIH cells at 36 h (**aI**) and 30 days (**aII**) of oncogene expression. Percent change in mitochondrial morphometric parameters during the early (36 h) and later (30 days) phases of neoplastic transformation compared with untransformed cells (MSCV): (**b**) mitochondrial volume, at 36 h: H-Ras_{12v} 123.4 ± 2.23%; at 30 days: H-Ras_{12v} 101.0 ± 0.94%. (**c**) Number of mitochondrial objects, at 36 h: H-Ras_{12v} 142.4 ± 3.48%; at 30 days: H-Ras_{12v} 96.0 ± 4.81%, (**d**) mitochondria–ER contact sites, at 36 h: H-Ras_{12v} 121.2 ± 1.99%; at 30 days: H-Ras_{12v} 102.0 ± 0.50%. (**e**) Measurements of the mitochondrial membrane potential in mock and H-Ras_{12v}-transformed 3T3NIH cells at 1.5 and 30 days of oncogene expression. The bars show the change in the TMRM fluorescence level before and after treatment with carbonyl cyanide *p*-trifluoromethoxyphenylhydrazone used to collapse the $\Delta\Psi$, expressed as the % change with respect to MSCV cells (at 36 h: H-Ras_{12v} 167.5 ± 13.1%; at 30 days: H-Ras_{12v} 170.7 ± 34.7%). (**f**) Mitochondrial Ca^{2+} uptake in permeabilized cells during the early and later phases of neoplastic transformation. The cells have been maintained in milieu containing thapsigargin (to ensure depletion of ER store) and ethylene glycol tetraacetic acid (EGTA; to ensure Ca^{2+}-free condition). Representative traces (**fI**,**II**) and percent change (**fIII**, at 36 h: H-Ras_{12v} 150.4 ± 10.43%; at 30 days: H-Ras_{12v} 151.9 ± 9.88%) are shown. Where indicated by '(Ca^{2+} 1 μM),' the medium was switched from IB/EGTA to IB/1 μM [Ca^{2+}]. Black trace, empty vector-expressing 3T3NIH cells; gray trace, H-Ras_{12v}-overexpressing cells. (**g**) Effects of oncogenic stress on superoxide production in H-Ras_{12v}-transformed 3T3NIH cells stained with the mitochondrial superoxide probe MitoSox. A representative plot (**gI**) and quantification of the percentage of cells positive for MitoSox staining (**gII**) during the early and later phases of neoplastic transformation are shown (at 36 h: MSCV + 13.8 ± 0.9% vs H-Ras_{12v} + 33.1 ± 2.5%; at 30 days: MSCV + 21.2 ± 0.3% vs H-Ras_{12v} + 41.5 ± 1.7%).

during the later phase of transformation. A drastic reduction in $[Ca^{2+}]_m$ and a lack of mitogenesis were evident in fully transformed cells, although an increased $\Delta\Psi$ coupled to a major mitochondrial Ca^{2+} affinity and ROS production was maintained. The different mitochondrial behaviors observed at different time points during H-Ras_{12v} expression could underlie the changes in the bioenergetic profile and altered apoptotic capacity.

Paradoxically, the results described above show that $[Ca^{2+}]_m$ reduction is unrelated to higher $\Delta\Psi$ in fully transformed fibroblasts, suggesting a putative alteration upstream of mitochondria, such as intracellular Ca^{2+} depletion. To investigate this possibility, an aequorin Ca^{2+} probe and the Ca^{2+} indicator Fura-2-acetoxymethylester (Fura-2/AM) were used to investigate cytosolic agonist-dependent responses and basal intracellular Ca^{2+} concentrations ($[Ca^{2+}]_i$), respectively.

In Figure 3a, the $[Ca^{2+}]_c$ was not changed in the first hours after H-Ras_{12v} induction compared with control, confirming a specific mitochondrial effect of H-Ras_{12v} on Ca^{2+} signaling. In pre-transformed and later transformed cells, the cytosolic Ca^{2+} responses were significantly reduced ($\sim$20 and $\sim$50%, respectively) like the mitochondrial Ca^{2+} responses. These data confirm not only the direct involvement of the mitochondria in the first step of transformation but also an extensive intracellular Ca^{2+} content modification in the later phases of transformation. To test the hypothesis that the mitochondria were deprived of its preferential ion, we investigated the basal $[Ca^{2+}]_i$ using Fura-2/AM (Figure 3c). In agreement with the cytosolic aequorin data, the basal $[Ca^{2+}]_i$ is markedly lower in H-Ras_{12v}-transformed fibroblasts than in control. The dramatic reduction of basal $[Ca^{2+}]_i$ in pre- and later H-Ras_{12v}-transformed cells is consistent with mitochondrial and cytosolic Ca^{2+} decreases. These experiments indirectly confirm the effects of H-Ras_{12v} on mitochondria in the first stages of tumorigenesis. The effects of oncogene expression on cytosolic and basal Ca^{2+} content observed in transformed 3T3NIH were confirmed in PML-null, p53-null and E1a-overexpressing MEFs (Figures 3d, e and Tables 2 and 3). Therefore, the tumoral phenotypes promoted by H-Ras_{12v} show similar Ca^{2+} dynamics that seem to be independent by specific tumor-suppressor deletions or by overexpression of specific oncogenes.

The differences in basal $[Ca^{2+}]_i$ between control and H-Ras_{12v}-transformed cells were almost abolished in cells cultured in Ca^{2+}-free medium, suggesting as $[Ca^{2+}]_i$ depletion is due to altered PM Ca^{2+} permeability (Figure 3f). The $[Ca^{2+}]_i$ depends on Ca^{2+} transport across the PM through the systems of Ca^{2+} entry and Ca^{2+} extrusion. It has been reported that the oncogene Bcl-2 can influence the $[Ca^{2+}]_i$, regulating the Ca^{2+} efflux effector PMCA, to determine the cellular fate.[35] Using Fura-2/AM dye, we have measured the Ca^{2+} influx and Ca^{2+} efflux responses in control and fully transformed fibroblasts. In according to the protocols reported in 'Materials and methods' section, the Ca^{2+} influx in H-Ras_{12v}-transformed cells was significantly reduced ($\sim$45%) compare with control cells (Figure 3g). Whereas, no differences in Ca^{2+} efflux rate (Figure 3hI) and time (Figure 3hII) have been detected, suggesting that no alterations on Ca^{2+} extrusion pathways are involved. The Ca^{2+} extrusion experiments were performed in Ca^{2+}-free medium to exclude the oncogenic effects on Ca^{2+} influx response, as shown in Figures 3f, g. The downregulation of intracellular Ca^{2+} is a peculiar effect of H-Ras-dependent tumor maintenance. To understand whether $[Ca^{2+}]_i$ might be considered a major factor in oncogenic transformation, we forced a Ca^{2+} influx in transformed cells by preconditioning with high external Ca^{2+} concentration ($[Ca^{2+}]$ 10 mM). A higher extracellular $[Ca^{2+}]$ should increase the mitochondrial Ca^{2+} uptake and $[Ca^{2+}]_c$ after agonist stimulation. This prediction was confirmed: preconditioned H-Ras_{12v}-transformed cells showed increases in mitochondrial and cytosolic responses (almost 30% in mitochondria and 15% in the cytosol) compared with fully transformed fibroblasts without preconditioning (Figure 4a). The higher basal $[Ca^{2+}]$ promoted by the increased external $[Ca^{2+}]$ affected the growth capacity of the cells, see Figure 4b. Indeed, the observed reduction in colony formation (Figure 4c) confirmed the inability of preconditioned H-Ras_{12v}-transformed cells to grow without attachment. The reduction in the cell number, as shown by clonogenic assays, suggests that the sensitivity to apoptosis is restored in these cells. After 7 days of incubation with 10 mM of extracellular $[Ca^{2+}]$, the H-Ras_{12v}-transformed cells showed a reactivation of the apoptotic machinery, confirmed by increase in cleaved form of apoptotic marker PARP (Figure 4d). The same scenario on Ca^{2+} signaling was evident also in control cells cultured in high external $[Ca^{2+}]$, where preconditioned control cells presented an increased basal cytosolic $[Ca^{2+}]$ (Supplementary Figure 1A) and in cytosolic Ca^{2+} response after stimulation with agonist (Supplementary Figure 1B). This has potentiated the growth capacity of the cells (Supplementary Figure 1C), inhibiting the apoptotic cell death (Supplementary Figure 1D).

Although most fundamental biological processes require the release of Ca^{2+} from the ER, the influx of external Ca^{2+} is also essential to sustain many biological processes. The Ca^{2+} transport systems in the PM are critical not only for refilling of internal ER stores but also for the regulation and fine tuning of biological responses.

Because H-Ras_{12v} alters the basal $[Ca^{2+}]_i$ and because this change is sustained by the activity of several PM Ca^{2+}-regulators, we investigated the activity of the caveolae in response to H-Ras_{12v} transformation.

First, we used MEFs wild type (wt) and 3T3NIH-expressing H-Ras_{12v} to confirm that expression of caveolin-1 is regulated by oncogenic stimuli (Figure 5a). We observed strikingly different levels of caveolin-1; in oncogenic-induced senescent cells (MEFs wt), the caveolin-1 level may be upregulated by an oncogenic stimulus,[36] whereas in 3T3NIH, neoplastic progression is strictly linked to caveolin-1 downregulation.[37] In the later transformation phase, we observed not only an alteration in caveolin-1 expression but also a difference in its intracellular redistribution. Figure 5b shows that, in non-transformed fibroblasts, caveolin-1 was redistributed to the PM and co-localized with endogenous H-Ras, as shown in the 'contact sites' image. Conversely, fully H-Ras_{12v}-transformed fibroblasts demonstrated caveolin-1 endomembrane accumulation. In support of immunofluorescence analysis, biochemical sub-membrane localization of caveolin-1 has been reported in Figure 5c, where non-transformed and H-Ras_{12v}-transformed cells were fractioned by OptiPrep gradient centrifugation. Western blot of each fractions showed that caveolin-1 was less localized in the low-density membrane fractions in fully transformed than control cells. This was then confirmed by western blot analysis of isolated lipid rafts, as shown in Figure 5d, where it is also evident as in H-Ras_{12v}-transformed cells caveolin-1 is redistributed to microsomes. Alternatively, oncogenes could regulate caveolin-1 activity through protein colocalization at the endomembrane, which would allow the retention of caveolin-1 and facilitate its degradation.[38]

It is logical to speculate that the decrease in the basal $[Ca^{2+}]_i$ during cell transformation could be mediated by the downregulation and redistribution of caveolin-1. To explore this possibility, we transduced H-Ras_{12v}-transformed cells with caveolin-1. We then measured the basal $[Ca^{2+}]_i$ and Ca^{2+} influx capacity after caveolin-1 reintroduction at 36 h and after extended re-expression. In Figure 5e, caveolin-1 re-expression favors the internalization of Ca^{2+}, producing a higher basal $[Ca^{2+}]_i$ than that observed in transformed cells (Figure 5eII and eIV). This higher concentration is sustained by an increased Ca^{2+} influx when the caveolin-1-reintroduced transformed cells are exposed to 2 mM of $[Ca^{2+}]$ (Figure 5cIII). Our results indicate that the reintroduction of caveolin-1 is essential for the refilling of the intracellular Ca^{2+} and the enhancement of the Ca^{2+} influx. In

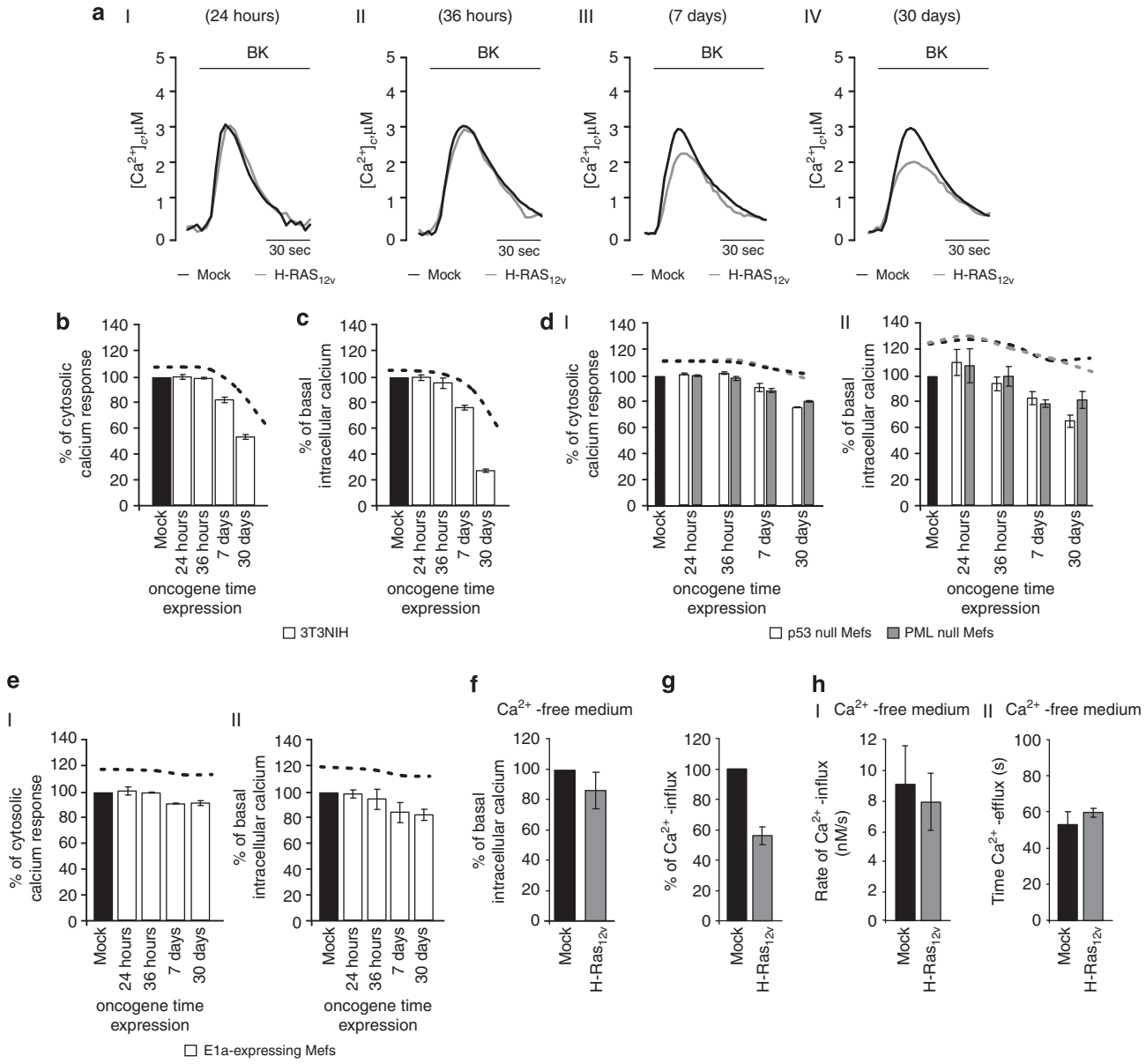

Figure 3. Oncogenic H-Ras$_{12v}$-induced transformation is sustained through the alteration of intracellular Ca^{2+} homeostasis. (**a**) [Ca^{2+}] measurements in the cytosol of control cells (mock) and H-Ras$_{12v}$-expressing cells at different time points after stimulation with 1 μM bradykinin: (**I**) at 24 h of expression: $[Ca^{2+}]_c$ in mock cells: 3.03 ± 0.27 μM vs H-Ras$_{12v}$: 3.02 ± 0.19 μM; (**II**) at 36 h of expression: $[Ca^{2+}]_c$ in mock cells: 2.94 ± 0.13 μM vs H-Ras$_{12v}$: 2.92 ± 0.18 μM; (**III**) at 7 days of expression: $[Ca^{2+}]_c$ in mock cells: 2.75 ± 0.10 μM vs H-Ras$_{12v}$: 2.22 ± 0.06 μM; (**IV**) at 30 days of expression: $[Ca^{2+}]_c$ in mock cells: 2.92 ± 0.14 μM vs H-Ras$_{12v}$: 1.96 ± 0.15 μM. (**b**) Histograms representing the cytosolic Ca^{2+} response, expressed as the percent change with respect to empty vector-expressing cells at different time points (at 24 h of oncogene expression: 100.8 ± 1.8%, at 36 h: 99.6 ± 0.4%, at 7 days: 81.2 ± 2.3% and at 30 days: 66.7 ± 6.1%). (**c**) Basal concentrations of free intracellular Ca^{2+} in mock and H-Ras$_{12v}$-expressing 3T3NIH cells during tumoral progression. $[Ca^{2+}]_i$ was measured using Fura-2AM on an inverted fluorescence microscope (Zeiss Axiovert 200) as described in the Materials and methods section. The bars show the percent reduction in intracellular Ca^{2+} content with respect to the control cells at four time points (at 24 h of oncogene expression: 99.3 ± 2.1%, at 36 h: 94.9 ± 4.3%, at 7 days: 76.1 ± 1.9% and at 30 days: 26.6 ± 1.3%). (**d**) Percent change in the cytosolic Ca^{2+} response (**I**) and basal Ca^{2+} content (**II**) in H-Ras$_{12v}$-transformed p53/PML-*null* cells and (**e**) E1a-expressing fibroblasts, compared with control cells. All data are summarized in Tables 2 and 3. (**f**) Basal $[Ca^{2+}]_i$ in mock and H-Ras$_{12v}$-transformed 3T3NIH cultured in Ca^{2+}-free medium. $[Ca^{2+}]_i$ was measured in Ca^{2+}-free KRB using Fura-2AM as described in the Materials and methods section. The bars show the percent variation in intracellular Ca^{2+} content with respect to the mock cells (H-Ras$_{12v}$: 84.3 ± 14.7%, $P < 0.338$). (**g**) Percentage Ca^{2+} influx response in H-Ras$_{12v}$-transformed 3T3NIH cells compare with mock cells expressed as 100%. The cells were before treated with BK (1 μM) and thapsigargin (2 μM) in order to completely empty the ER Ca^{2+} stores, then the extracellular [Ca^{2+}] was increased to 2 mM, which induced rapid Ca^{2+} influx (H-Ras$_{12v}$: 54.8 ± 5.8%). (**h**) Rate of intracellular Ca^{2+} extrusion (**I**) and time (**II**) of reduction in $[Ca^{2+}]_i$ in mock and H-Ras$_{12v}$-transformed fibroblasts. The data have been collected following the procedure described in 'Materials and methods' section (rate of Ca^{2+} efflux: MSCV 8.99 ± 2.6 nM/s vs H-Ras$_{12v}$ 8.05 ± 1.9 nM/s; time of Ca^{2+} efflux: MSCV 52.70 ± 7.4 s vs H-Ras$_{12v}$ 58.91 ± 2.6 s).

control cells, the overexpression of caveolin-1 increased the basal $[Ca^{2+}]_i$ (Supplementary Figure 2II) and Ca^{2+} influx capacity (Supplementary Figure 2III). These data suggest that caveolin-1 can directly regulate the Ca^{2+} influx machineries, without change their expression both in control and in transformed cells (Supplementary Figure 2B). At sustain of it, the pretreat-

Table 2. Percent change in the cytosolic Ca^{2+} response in H-Ras_{12v}-transformed p53/PML-*null* cells and E1a-expressing fibroblasts, compared with control cells

H-Ras_{12v}trasforming	T *24 h*	T *36 h*	T *7 days*	T *30 days*
p53 *null* MEF	101.3 ± 0.7	103.3 ± 1.0	90.8 ± 2.9	75.0 ± 0.4
PML *null* MEF	100.2 ± 0.7	98.1 ± 1.4	88.6 ± 1.4	80.2 ± 0.7
E1a-expressing MEF	99.6 ± 3.2	97.9 ± 0.1	− 90.0 ± 0.3	− 90.9 ± 1.6

Abbreviation: MEF, mouse embryonic fibroblast. In the table are summarized the data of Figures 3dI and el.

Table 3. Percent change in the basal Ca^{2+} content in H-Ras_{12v}-transformed p53/PML-*null* cells and E1a-expressing fibroblasts, compared with control cells

H-Ras_{12v}trasforming	T *24 h*	T *36 h*	T *7 days*	T *30 days*
p53 *null* MEF	109.2 ± 9.9	92.4 ± 5.1	81.3 ± 5.0	63.9 ± 4.5
PML *null* MEF	106.9 ± 14.3	98.9 ± 7.5	77.9 ± 2.6	80.0 ± 6.7
E1a-expressing MEF	97.8 ± 3.0	93.8 ± 7.7	83.5 ± 7.0	82.0 ± 3.9

Abbreviation: MEF, mouse embryonic fibroblast. In the table are summarized the data of Figures 3dII and ell.

ment with store-operated channel (SOC) channel inhibitors, SKF-96365 (10 μM), 2-aminoethoxydiphenyl borate (100 μM) and gadolinium chloride ($GdCl_3$, 1 mM) were able to contrast the caveolin-1's effect on basal $[Ca^{2+}]_i$ (Figure 5fI) and Ca^{2+} influx capacity (Figure 5fII). These data shed light on architectural and functional role of caveolin-1 in coordinate and control the mechanisms involved in Ca^{2+} influx.

Caveolin-1 reintroduction could favor a major Ca^{2+} release by the agonist-sensitive Ca^{2+} stores as a consequence of the increased Ca^{2+} filling of the ER lumen. This is confirmed by the mitochondrial and cytosolic Ca^{2+} responses, observed upon IP3 agonist stimulation, plotted in Figure 5gI and gII. The caveolin-1-reintroduced transformed fibroblasts exhibited an increase of ~20% in $[Ca^{2+}]_m$ and $[Ca^{2+}]_c$ compared with transformed cells after stimulation.

The Ca^{2+} recovery mediated by caveolin-1 re-expression can be associated with the suppression of the transformed phenotype. In fact, caveolin-1 reintroduction in H-Ras_{12v}-transformed cells compromises the cellular growth (Figure 5h) and significantly decreases both colony size and efficiency of colony formation; a reduction of ~40% in the colony formation is shown in Figure 5i.

Finally, we confirmed the activation of apoptosis following the re-expression of caveolin-1 in H-Ras_{12v}-transformed cells by evaluating the levels of cleaved PARP, as shown in Figure 5j.

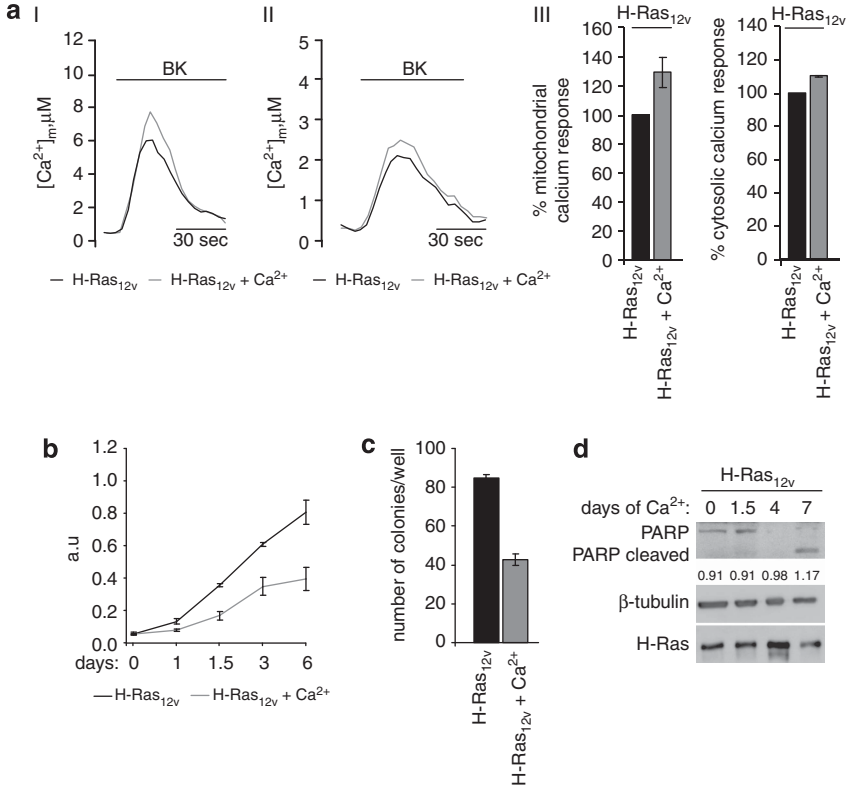

Figure 4. Preconditioning with higher external Ca^{2+} concentrations re-establishes the sensitivity of transformed cells to apoptosis. $[Ca^{2+}]_m$ (**aI**) and $[Ca^{2+}]_c$ (**aII**) increases were elicited by preconditioning fully H-Ras_{12v}-transformed cells with high (10 mM) external Ca^{2+} concentrations. The cells were stimulated with the IP3-dependent agonist bradykinin as indicated (**I**) $[Ca^{2+}]_m$ in H-Ras_{12v}: 5.96 ± 0.6 μM vs H-Ras_{12v} + Ca^{2+}: 7.71 ± 0.8 μM; $[Ca^{2+}]_c$ in H-Ras_{12v}: 2.18 ± 0.04 μM vs H-Ras_{12v} + Ca^{2+}: 2.36 ± 0.05 μM. (**aIII**) Histogram representing the percent change in the mitochondrial and cytosolic Ca^{2+} responses relative to non-preconditioned H-Ras_{12v}-transformed cells (mitochondria: 129.81 ± 10.9%; cytosol: 112.29 ± 0.7%). (**b**) Growth curves of preconditioned and non-preconditioned H-Ras_{12v}-transformed 3T3NIH cells (H-Ras_{12v}: T0: 0.067 ± 0.009, T1: 0.143 ± 0.015, T1.5: 0.363 ± 0.009, T3: 0.610 ± 0.012, T6: 0.803 ± 0.088 vs H-Ras_{12v} + Ca^{2+}: T0: 0.077 ± 0.003, T1: 0.097 ± 0.007, T1.5: 0.187 ± 0.027, T3: 0.363 ± 0.055, T6: 0.410 ± 0.080). (**c**) Soft agar colony formation assay of fully H-Ras_{12v}-transformed and preconditioned H-Ras_{12v}-transformed cells. Three independent assays were quantified (*n* of H-Ras_{12v} colonies: 85.3 ± 1.8; *n* of H-Ras_{12v} + Ca^{2+} colonies: 42.7 ± 2.7). (**d**) Western blot analysis of PARP cleavage in H-Ras_{12v}-transformed 3T3NIH cells preconditioned with high (10 mM) external Ca^{2+} concentrations. The PARP cleavage was quantified using densitometry, and the ratios of cleaved to uncleaved PARP are indicated. The results are representative of three independent experiments.

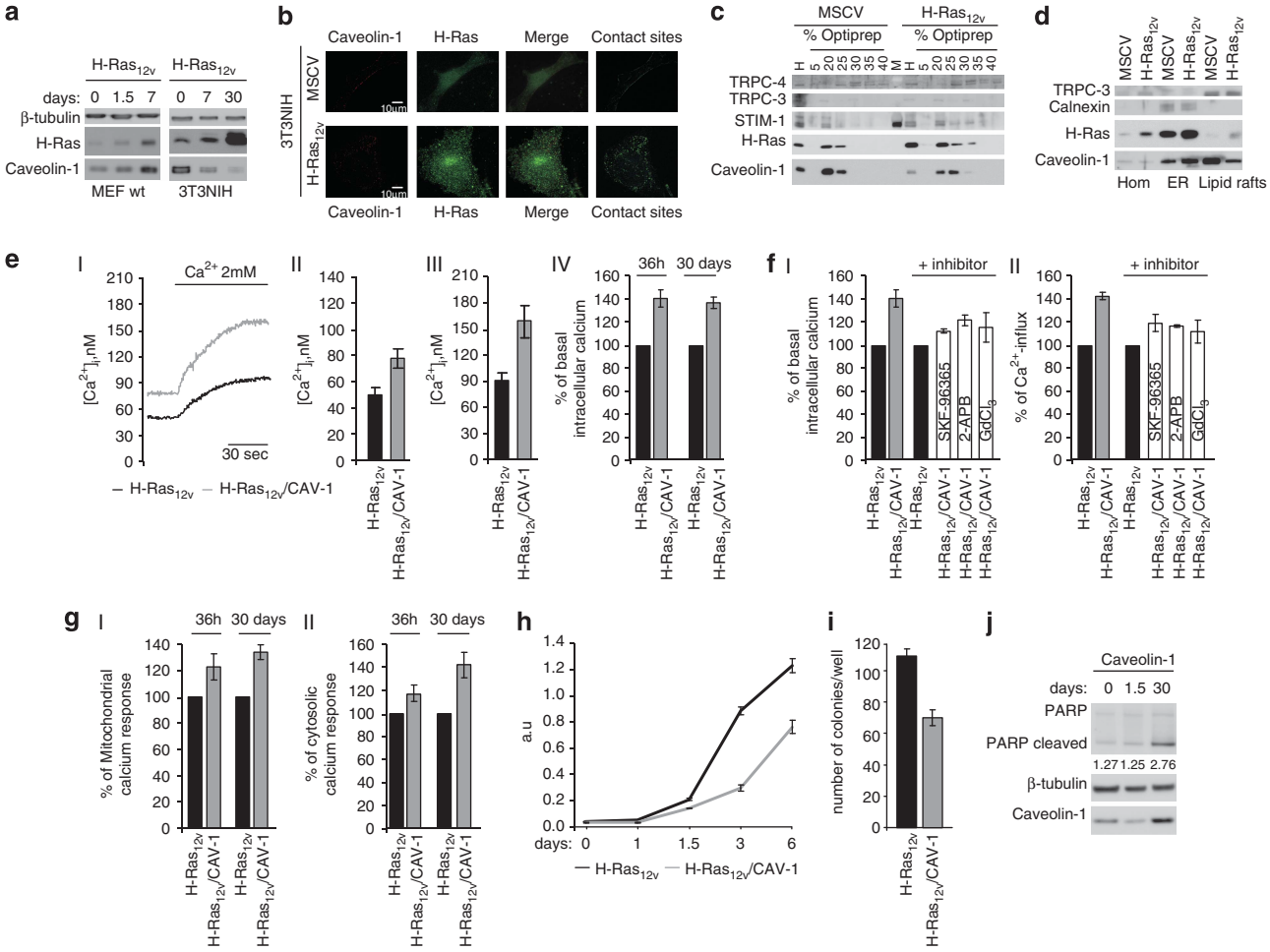

Figure 5. Caveolin-1 is a crucial regulator of intracellular Ca^{2+} and a direct link between the neoplastic phenotype and mitochondrial biology. (**a**) Time-dependent changes in caveolin-1 expression, detected by western blot, in H-Ras_{12v}-driven oncogenic senescent mouse fibroblasts (MEF wt) and H-Ras_{12v}-driven tumoral 3T3NIH cells. (**b**) Oncogenic Ras disrupts the caveolar structure by modifying intracellular caveolin-1 expression and localization. Immunofluorescence of H-Ras (green) and caveolin-1 (red) in control and fully H-Ras_{12v}-transformed cells. Co-localization analysis demonstrates specific contact sites between the two proteins examined, as reported in the inset ('contact sites'). (**c**) Sub-membrane localization of caveolin-1 and H-Ras in non-transformed and H-Ras_{12v}-transformed 3T3NIH cells fractioned by OptiPrep gradient centrifugation. Cell lysates were subjected to Triton X-100 extraction and OptiPrep density gradient separation. Six fractions and homogenates were collected and analyzed by western blot with specific antibodies. (**d**) Lipid rafts and ER redistribution of caveolin-1 and H-Ras in mock and H-Ras_{12v}-transformed 3T3NIH cells, through western blot analysis. (**e**) Basal concentrations of free intracellular Ca^{2+} and Ca^{2+} influx in H-Ras_{12v}-transformed cells, measured after caveolin-1 reintroduction. $[Ca^{2+}]_i$ changes were measured using Fura-2AM, as described in the Materials and methods section. (**eI**) Representative traces have been reported; where indicated, 2 mM $CaCl_2$ has been added to favor the Ca^{2+} influx. The bars show the mean of basal Ca^{2+} content (**eII**) and Ca^{2+} influx (**eIII**) in caveolin-1-reintroduced transformed cells with respect to H-Ras_{12v}-driven tumoral 3T3NIH cells. (**II**) Basal Ca^{2+} content: $[Ca^{2+}]_i$ in H-Ras_{12v}: 50.5 ± 7.3 nM vs H-Ras_{12v}/Cav-1: 77.7 ± 8.3 nM; (**III**) Ca^{2+} influx: $[Ca^{2+}]_i$ in H-Ras_{12v}: 92.6 ± 12.8 nM vs H-Ras_{12v}/Cav-1: 161.8 ± 26.3 nM. (**eIV**) The bars represent the percent change in basal intracellular Ca^{2+} concentrations in reintroduced caveolin-1-transformed 3T3NIH cells (36 h and 30 days of caveolin-1 expression) with respect to fully H-Ras_{12v}-transformed 3T3NIH cells (at 36 h of caveolin-1 expression: 142.3 ± 8.9%; at 30 days: 136.5 ± 4.8%). (**f**) Histograms representing the basal Ca^{2+} content (**I**) and Ca^{2+} influx response (**II**), expressed as the percent change with respect to inhibitors-treated H-Ras_{12v}-transformed cells at inhibitors-pretreated caveolin-1-reintroduced transformed cells. The data have been collected following the procedures described in the Materials and methods section (**II** Basal Ca^{2+} content: $[Ca^{2+}]_i$ no pretreated H-Ras_{12v}/Cav-1: 142.26 ± 8.9%; SKF-96365-treated H-Ras_{12v}/Cav-1 107.00 ± 1.5%; 2-aminoethoxydiphenyl borate (2-APB)-treated H-Ras_{12v}/Cav-1 120.73 ± 4.5%; $GdCl_3$-treated H-Ras_{12v}/Cav-1 116.50 ± 12.8%. **III** Ca^{2+} influx: $[Ca^{2+}]_i$ no pretreated H-Ras_{12v}/Cav-1: 144.41 ± 1.8%; SKF-96365-treated H-Ras_{12v}/Cav-1 119.06 ± 7.6%; 2-APB-treated H-Ras_{12v}/Cav-1 117.70 ± 1.4%; $GdCl_3$-treated H-Ras_{12v}/Cav-1 111.61 ± 10.0%). (**g**) Increases in $[Ca^{2+}]_m$ (**gI**) and $[Ca^{2+}]_c$ (**gII**) elicited by caveolin-1 reintroduction in fully H-Ras_{12v}-transformed cells. The experiments were performed at 36 h and 30 days of caveolin-1 expression, and the results are expressed as the percent change (mitochondrial Ca^{2+} response at 36 h of expression: 122.9 ± 9.9%; at 30 days: 133.7 ± 5.7%; cytosolic Ca^{2+} response at 36 h of expression: 116.1 ± 7.1%; at 30 days: 141.2 ± 11.2%). (**h**) Growth curves of H-Ras_{12v}-transformed 3T3NIH cells and caveolin-1-reintroduced cells (H-Ras_{12v}: T0: 0.023 ± 0.001, T1: 0.035 ± 0.003, T1.5: 0.190 ± 0.010, T3: 0.854 ± 0.030, T6: 1.194 ± 0.052 vs H-Ras_{12v}/Cav-1: T0: 0.016 ± 0.003, T1: 0.015 ± 0.001, T1.5: 0.123 ± 0.002, T3: 0.277 ± 0.025, T6: 0.735 ± 0.053). (**i**) Soft agar colony formation assay of fully H-Ras_{12v}-transformed and caveolin-1-reintroduced cells. Three independent assays were quantified (*n* of H-Ras_{12v} colonies: 112.0 ± 4.8; *n* of H-Ras_{12v}/Cav-1 colonies: 72.0 ± 5.2). (**j**) Western blot analysis of PARP cleavage in H-Ras_{12v}-transformed 3T3NIH where it has been reintroduced caveolin-1. Quantification of PARP cleavage detected was performed using densitometry and ratios of cleaved to uncleaved PARP, as indicated in figure. The results are representative of three independent experiments.

DISCUSSION

Much attention has been devoted to understand the complexity of Ca^{2+} signaling. It is known that a rise in $[Ca^{2+}]_c$ allows the transfer of information conveyed by a variety of extracellular signals and decodes these signals into diverse intracellular biological effects.[39] This pleiotropic signaling potentially allows the same signaling molecule to induce different effects in the same cell, depending on the degree of spatio-temporal complexity of the signal. In turn, a high degree of complexity is achieved through the large diversity of the molecular elements controlling Ca^{2+} homeostasis.

The results of this work demonstrate that intracellular Ca^{2+} homeostasis changes after the induction of H-Ras_{12v} and describe the temporal relationship between oncogene expression and mitochondrial physiology.

These results also demonstrate the role of caveolin-1, a protein that is important for tumor maintenance, in the regulation of Ca^{2+} homeostasis.

To date, little research has aimed to understand the mechanism or role of caveolin-1 in Ca^{2+} influx in the context of cancer biology. Many oncogenes induce a marked reduction in caveolin-1 expression, resulting in the loss of caveolae from transformed cells,[40–45] this downregulation is typically correlated with increased proliferation and anchorage-independent cell growth, but in certain cancers, caveolin-1 expression is advantageous for cancer progression and promotes metastasis.[46,47] Understanding the role of caveolin-1 in cancer maintenance requires knowledge about the effects of caveolin-1 on the regulation of pathways essential for the onco-bioenergetic and death responses. Caveolin-1 is a tumor suppressor that prevents cell transformation[48] promoting cell cycle arrest[49] in cyclin D1[50] and $p53/p21^{WAF1/Cip1}$-dependent mechanism.[51] The role of caveolin-1 as a tumor promoter or suppressor is strongly determined by the specific cellular context, in fact, caveolin-1 acts as a scaffolding protein to concentrate and functionally regulate signaling molecules such as Ca^{2+}-signaling members or Ras.[52] Furthermore, caveolin-1 is essential for Ca^{2+} entry into endothelial cells and governs the localization and protein–protein interactions between the transient receptor channels C4 and C1 (TRPC)[53] and between the inositol trisphosphate receptor-1 and TRPC-3 in cerebral artery smooth muscle cells.[54]

Our results connect this tumor suppressor to the core mechanism of Ca^{2+}-dependent pathway of apoptosis and show that it participates in the regulation of critical mitochondrial functions. This effect was demonstrated by the reintroduction of caveolin-1 into fully transformed fibroblasts, which favors intracellular Ca^{2+} refilling and contributes to sensitizing the mitochondria, thus increasing the possibility that some stimulatory input to the cell reaches the threshold required to initiate the apoptotic Ca^{2+} wave. The results shown in Figure 5 demonstrate that caveolin-1 increases mitochondrial Ca^{2+} uptake (an initial step of the intrinsic apoptotic pathway) and strongly support this model. The temporal relationship between oncogene expression and the downregulation of caveolin-1 sheds light on the escape signaling route that allows cancer cells to avoid apoptosis. In this study, we have shown that compartmentalized H-Ras_{12v} sustains tumorigenesis and tumor maintenance through the altered intracellular Ca^{2+} homeostasis promoted by the loss of caveolin-1 functionality and expression. The observation that caveolin-1 is directly engaged in this process furthers our understanding of the function of this important tumor suppressor and highlights the relevance of mitochondrial Ca^{2+} homeostasis in cancer-related apoptosis.

The focus on Ca^{2+} signaling by Ras is interesting and could be an important emerging area of cancer research. The precise localization of the oncogene in two strategic Ca^{2+}-regulating districts, PM-associated membranes (PAMs, the putative PM/ER contact sites) and MAM, as reported in Figure 1, suggests a cooperation between PM, ER and mitochondria that is essential for Ca^{2+} signaling and the maintenance of Ca^{2+} homeostasis in cancer progression. These specific intracellular locations define the sites of PM/ER/mitochondria juxtaposition that control the Ca^{2+} flux between these organelles. Our study suggests a new mechanism of escape from Ca^{2+}-mediated apoptotic signaling, whereby H-Ras_{12v} accumulation at the PAM and MAM alters Ca^{2+} dynamics and acts as effector of mitochondrial-mediated transformation. The role of mitochondria in Ca^{2+} signaling was re-evaluated after it was shown that these organelles not only undergo changes in $[Ca^{2+}]$ under various physiological and pathological conditions but also have an important role in decoding the Ca^{2+} signal, that is, determining the final cellular outcome.[55] Although $[Ca^{2+}]_m$ is of major pathophysiological interest, few molecular details are currently available that allow the mitochondria to come into close contact with the ER Ca^{2+} store. Little, if anything, is known about the regulatory mechanisms that control the efficiency of mitochondrial Ca^{2+} uptake and Ca^{2+} homeostasis in a tumoral environment. Warburg observed that cancer cells favor glycolysis even in the presence of high oxygen, and the 'Warburg effect' remains puzzling, today. Recently, several findings have challenged the Warburg hypothesis and proposed a different role for the mitochondria in cancer, demonstrating that the ability of melanoma cells to form tumors and to induce metastasis is dependent on functional mitochondria.[56] A novel model to explain tumor metabolism, termed 'The Reverse Warburg effect' was formulated.[57] This model proposed that cancer-associated fibroblasts secrete high levels of energy-rich metabolites that are directly absorbed by tumor cells and are used for efficient ATP production via oxidative phosphorylation.[58]

As shown in Figure 2, the expression of H-Ras_{12v} promotes precise mitochondrial changes to raise the mitochondrial sensitivity, predisposing the organelle to be more responsive to cellular demands. Our data suggest that the increases in mitochondrial potential, mitochondrial Ca^{2+} affinity, the volume and distribution of the mitochondrial network represent compensatory responses to a greater energy demand and provide the cells with a way to promote protein synthesis and growth during transformation. This mitochondrial hyperactivity is not sustainable for a long period of time, as the cells degenerate quickly due to an enhanced mitochondrial sensitivity to apoptotic stimuli. The mitochondrial oncogenic stress leads, through an as-yet poorly defined mechanism, to the overproduction of ROS, which in turn damages the mitochondria. Under these conditions, autophagy may prevent major respiratory chain dysfunction by ensuring the preferential elimination of dysfunctional organelles through the quality control process termed 'mitophagy'.[59]

The modulation of mitochondrial functions by the oncogene involves the capability of the seizure of Ca^{2+} ion, through the modulation of the activity of the Ca^{2+}-regulator caveolin-1, which is distributed throughout the PAM and MAM.[60] The results shown in Figure 4 provide additional support for this model, showing that preconditioning with high external $[Ca^{2+}]$ re-establishes sensitivity to apoptosis in transformed cells. These results also demonstrate that transformed cells and mitochondria are highly susceptible to Ca^{2+}-dependent apoptotic stimuli.

In conclusion, we demonstrated that: (i) intracellular Ca^{2+} signaling has an important role in the tumor formation and maintenance promoted by compartmentalized H-Ras; (ii) caveolin-1 is a crucial regulator of Ca^{2+} PM-microdomains and of store-operated Ca^{2+}-entry; (iii) caveolin-1 enhances Ca^{2+} uptake into mitochondria, thereby promoting its tumor-suppressor activity; (iv) the Cav-1/H-Ras_{12v} axis contributes to mitochondrial apoptotic failure and induces the neoplastic phenotype, indicating a direct link between Ca^{2+} regulation and mitochondrial biology in cancer; (v) H-Ras_{12v} compromises the cooperation

between the PAM and MAM, which is a one key step of the phenotypic conversion that occurs during tumor formation.

MATERIALS AND METHODS

Cell culture and viral transduction

Cells were maintained at 37 °C under 5% CO_2. 3T3NIH-expressing H-Ras_{12v}, caveolin-1 and empty vector were maintained in Dulbecco's modified Eagle's medium (DMEM) containing 10% fetal bovine serum, 100 U/ml penicillin and streptomycin. Stable cell lines were generated by retroviral transduction and selection for puromycin and hygromycin resistance, and maintained under 0.2 μg/ml of puromycin or 5 μg/ml hygromycin, respectively. For aequorin experiments, the cells were transducted with adenoviral aequorin-targeted probes (mtAEQ and cytAEQ), the measures were performed 36 h after transduction.

Growth curve assay

Cell growth curves were generated by crystal violet staining. Cells were seeded with low cell density (10 000 per 12 wells) in triplicates and allowed to grow for 6 days. At 24 h, 36 h, 3 and 6 days, cells were washed with phosphate-buffered saline, fixed with 4% paraphormaldehyde and stained with 0.1% crystal violet. Crystal violet was dissolved with 1 mol/l acetic acid and A_{595} was measured.

Soft-agar assays

Approximately 10 000 cells were suspended in 2 ml of agar (0.3% agar in DMEM) and layered over a solidified cushion of 0.6% agar in DMEM. Individual macroscopic colonies were counted after 4 weeks of growth.

Aequorin measurements

For the mtAEQ or cytAEQ measurements, the cells were incubated with 2 μM coelenterazine for 1–2 h in DMEM and then transferred to the perfusion chamber. The thermostated chamber is located in close proximity of a low-noise photomultiplier. All the experiments have been performed with 1 mM external $[Ca^{2+}]$ or only where indicated, the cells were maintained in Ca^{2+}-free medium. Agonist (Bradykinin 1 μM or ATP 100 μM, Sigma-Aldrich, St Louis, MO, USA) and other drugs were added to the same medium, as specified in figure legends. For the experiments with permeabilized cells, intracellular medium containing 20 μM digitonin and thapsigargin were perfused. Buffer containing ethylene glycol tetraacetic acid-buffered $[Ca^{2+}]$ of 1 μM was added to induce the mitochondrial Ca^{2+} uptake. All experiments were terminated lysing the cells with 100 μM Triton in a hypotonic Ca^{2+}-containing solution (10 mM $CaCl_2$). The output of the discriminator was captured by a Thorn-EMI photon, the data were calibrated off-line into $[Ca^{2+}]$ values, using a computer algorithm based on the Ca^{2+}-response curve of wild-type and mutant aequorins.[32] Statistical data are presented as mean ± s.e.

Fura-2/AM measurements

The intracellular basal $[Ca^{2+}]_i$, Ca^{2+} influx and Ca^{2+} efflux responses were evaluated using the Ca^{2+} indicator Fura-2-acetoxymethyl-ester (Fura-2/AM; Molecular Probes, Eugene, OR, USA). Briefly, cells were incubated in medium supplemented with 2.5 μM Fura-2/AM for 30 min, washed with krebs ringer buffer (KRB) and placed in thermostated incubation chamber on stage of an inverted fluorescence microscope (Zeiss Axiovert-200, Carl Zeiss AG, Oberkochen, Germany). All the experiments have been performed with 1 mM external $[Ca^{2+}]$, or only where indicated, the cells were maintained in Ca^{2+}-free medium. Dynamic video imaging was performed using the Metafluor-software (Universal Imaging Corporation, Bedford Hills, NY, USA). Fluorescence was measured every 100 ms and the $[Ca^{2+}]_i$ was calculated by the ratio method using the equation: $[Ca^{2+}]_c = Kd\ (R–Rmin)/(R–Rmax) \times Sf2/Sf1$.

To monitor the Ca^{2+} influx response, the cells were before treated with bradykinin (BK) (1 μM) and thapsigargin (2 μM), a specific inhibitor of Ca^{2+} pumps in the ER (SERCA), in order to completely empty the ER Ca^{2+} stores, then the extracellular $[Ca^{2+}]$ was increased to 2 mM, which induced rapid influx of Ca^{2+} to the cytosol. Although, to monitor the Ca^{2+} efflux response, we measured the rate and time of $[Ca^{2+}]_i$ reducing during the complete inhibition of Ca^{2+} uptake into the ER. The cells exposed to a Ca^{2+}-free solution were treated with thapsigargin, in this case the Ca^{2+} extrusion was the only process responsible for recovery. The extracellular Ca^{2+} concentration was then increased to 2 mM, after a stable $[Ca^{2+}]_i$ plateau had been attained, the $[Ca^{2+}]_i$ declined until the baseline level. The rate of decline of $[Ca^{2+}]_i$ and time must reflect the rate and the time of Ca^{2+} extrusion. Calcium extrusion rates ($d[Ca^{2+}]_i/dt$) and time were calculated and shown as response mean for each experimental condition.

Analysis of mitochondrial morphology

The cells were seeded on 24-mm coverslips. The cells were imaged with a laser-scanning confocal Zeiss LSM-510 (Carl Zeiss AG). To obtain the best object reality, images were next deconvolved using the open source software Fiji. Once reconstructed, a mitochondrial and ER mask were manually chosen to obtain a binarized image of overlapping areas. The resulting areas were described in number and volume, using the three-dimensional object counter, available in Fiji.

Mitochondrial membrane potential assay

The cells were plated in 6-well plates. The $\Delta\Psi$ was measured using the fluorescent dye TMRM. Briefly, the dye was loaded onto cells at 100 nM in KRB, placed at 37 °C for 20 min and measured on laser-scanning confocal Zeiss LSM-510. In order to control, each experiment is treated with 10 μM carbonylcyanide-3-chlorophenylhydrazone, which collapses the $\Delta\Psi$. All data are expressed as % of the total TMRM fluorescence minus the carbonylcyanide-3-chlorophenylhydrazone -treated TMRM fluorescence.

Detection of mitochondrial ROS

For the determination of mitochondrial superoxide by flow cytometry, the measurements were carried out using FAScalibur (Becton, Dickinson and Company, Franklin Lakes, NJ, USA). Cells were then incubated with MitoSOX-Red indicator (Invitrogen, Life Technologies Ltd, Paisley, UK) for 30 min and washed. In this study, the data were presented in the FL2-channel. Cell debris as represented by distinct low forward and side scatter were gated out for analysis. The data presented by histogram of % of mean intensity of MitoSOX fluorescence.

Gradient analysis and lipid rafts isolation

Adherent cells were washed twice in phosphate-buffered saline, lysed with 2 ml of extraction buffer (20 mM Tris–HCl, pH 7.4, NaCl 150 mM, EDTA 1 mM) supplemented with 1% Triton X-100 and a protease inhibitor mixture. Lysates were scraped from the flasks, sheared by 20 passages through a 22-gauge needle, left for 20 min before mixing with OptiPrep density gradient medium (final concentration, 40% (v/v)), and placed at the bottom of a 12-ml ultracentrifuge tube. A Optiprep gradient was formed by overlaying 2 ml of 35, 30, 25, 20% Optiprep and 2 ml of 5% Optiprep (prepared by dilution of OptiPrep in extraction buffer). Gradients were ultracentrifuged at 100 000 *g* for 4 h in a SW40 rotor (Beckman Coulter s.r.l., Milano, Italy). A distinct Triton X-100-insoluble whitish band that floated to the 5–30% interface was designated as the detergent-resistant membrane fractions. The last 2 ml of the gradient tube were designated as the soluble fraction. The whole procedure was performed at 0–4 °C. Detergent-resistant membrane and soluble fractions were collected and subjected to western blot analysis.

Immunoblot analysis

The cell lysates were prepared in non-denaturing lysis buffer and loaded on a Novex NuPage precast gel (Invitrogen) and transferred onto nitrocellulose membranes. Isotype-matched, horseradish peroxidase-conjugated secondary antibodies (Santa Cruz Biotechnology, Santa Cruz, CA, USA) were used, followed by detection by chemiluminescence (Thermo Fisher Scientific Inc., Waltham, MA, USA), using ImageQuant LAS 4000 (GE Healthcare, Buckinghamshire, UK). Membranes were probed for desired proteins using specific primary antibodies: H-Ras antiserum (Novus Biologicals, Littleton, CO, USA), β-tubulin (Sigma), IP3-Receptor (Becton, Dickinson and Company), Sigma-1R (Sigma), Calnexin (Santa Cruz Biotechnology), VDAC (AbCam), caveolin-1 (AbCam, Cambridge, UK), TRPC-1 (Santa Cruz Biotechnology), TRPC-3 (Santa Cruz Biotechnology), TRPC-4 (Santa Cruz Biotechnology), Orai-1 (Santa Cruz Biotechnology), STIM-1 (Santa Cruz Biotechnology) and PARP (Cell Signalling, Danvers, MA, USA) in according to standard procedures.

CONFLICT OF INTEREST

The authors declare no conflict of interests.

ACKNOWLEDGEMENTS

This research was supported by: the Italian Ministry of Health to AR. SP is supported by a FISM (Fondazione Italiana Sclerosi Multipla) research fellowship (2012/B/11), whereas SM by FIRC (Fondazione Italiana Ricerca sul Cancro) fellowship. PP is financed by Italian Association for Cancer Research (AIRC), Telethon (GGP09128 and GGP11139B), local funds from the University of Ferrara, the Italian Ministry of Education, University and Research (COFIN, FIRB and Futuro in Ricerca), the Italian Cystic Fibrosis Research Foundation and Italian Ministry of Health.

REFERENCES

1 Malumbres M, Barbacid M. RAS oncogenes: the first 30 years. *Nat Rev* 2003; **3**: 459–465.
2 Downward J. Targeting RAS signalling pathways in cancer therapy. *Nat Rev* 2003; **3**: 11–22.
3 Chin L, Tam A, Pomerantz J, Wong M, Holash J, Bardeesy N *et al.* Essential role for oncogenic Ras in tumour maintenance. *Nature* 1999; **400**: 468–472.
4 Weinstein IB, Joe A. Oncogene addiction. *Cancer Res* 2008; **68**: 3077–3080 discussion 80.
5 Warburg O, Wind F, Negelein E. The metabolism of tumors in the body. *J General Physiol* 1927; **8**: 519–530.
6 Gough DJ, Corlett A, Schlessinger K, Wegrzyn J, Larner AC, Levy DE. Mitochondrial STAT3 supports Ras-dependent oncogenic transformation. *Science (New York, NY* 2009; **324**: 1713–1716.
7 Hu Y, Lu W, Chen G, Wang P, Chen Z, Zhou Y *et al.* K-ras(G12V) transformation leads to mitochondrial dysfunction and a metabolic switch from oxidative phosphorylation to glycolysis. *Cell Res* 2012; **22**: 399–412.
8 Gogvadze V, Orrenius S, Zhivotovsky B. Mitochondria in cancer cells: what is so special about them? *Trends Cell Biol* 2008; **18**: 165–173.
9 Kroemer G, Pouyssegur J. Tumor cell metabolism: cancer's Achilles' heel. *Cancer Cell* 2008; **13**: 472–482.
10 Giorgi C, Baldassari F, Bononi A, Bonora M, De Marchi E, Marchi S *et al.* Mitochondrial Ca(2+) and apoptosis. *Cell Calcium* 2012; **52**: 36–43.
11 Ralph SJ, Rodriguez-Enriquez S, Neuzil J, Saavedra E, Moreno-Sanchez R. The causes of cancer revisited: "mitochondrial malignancy" and ROS-induced oncogenic transformation - why mitochondria are targets for cancer therapy. *Mol Aspects Med* 2010; **31**: 145–170.
12 Clapham DE. Calcium signaling. *Cell* 2007; **131**: 1047–1058.
13 Pinton P, Ferrari D, Rapizzi E, Di Virgilio F, Pozzan T, Rizzuto R. The Ca2+ concentration of the endoplasmic reticulum is a key determinant of ceramide-induced apoptosis: significance for the molecular mechanism of Bcl-2 action. *EMBO J* 2001; **20**: 2690–2701.
14 Liu X, Hajnoczky G. Ca2+-dependent regulation of mitochondrial dynamics by the Miro-Milton complex. *Int J Biochem Cell Biol* 2009; **41**: 1972–1976.
15 Giorgi C, Agnoletto C, Bononi A, Bonora M, De Marchi E, Marchi S *et al.* Mitochondrial calcium homeostasis as potential target for mitochondrial medicine. *Mitochondrion* 2012; **12**: 77–85.
16 Peng TI, Jou MJ. Oxidative stress caused by mitochondrial calcium overload. *Ann NY Acad Sci* 2010; **1201**: 183–188.
17 Berridge MJ, Lipp P, Bootman MD. The versatility and universality of calcium signalling. *Nat Rev Mol Cell Biol* 2000; **1**: 11–21.
18 Simons K, Toomre D. Lipid rafts and signal transduction. *Nat Rev Mol Cell Biol* 2000; **1**: 31–39.
19 Thomas CM, Smart EJ. Caveolae structure and function. *J Cell Mol Med* 2008; **12**: 796–809.
20 Razani B, Schlegel A, Lisanti MP. Caveolin proteins in signaling, oncogenic transformation and muscular dystrophy. *J Cell Sci* 2000; **113**(Pt 12): 2103–2109.
21 Williams TM, Lisanti MP. The Caveolin genes: from cell biology to medicine. *Ann Med* 2004; **36**: 584–595.
22 Patel HH, Murray F, Insel PA. Caveolae as organizers of pharmacologically relevant signal transduction molecules. *Annu Rev Pharmacol Toxicol* 2008; **48**: 359–391.
23 Fujimoto T. Calcium pump of the plasma membrane is localized in caveolae. *J Cell Biol* 1993; **120**: 1147–1157.
24 Fujimoto T, Nakade S, Miyawaki A, Mikoshiba K, Ogawa K. Localization of inositol 1,4,5-trisphosphate receptor-like protein in plasmalemmal caveolae. *J Cell Biol* 1992; **119**: 1507–1513.
25 Jorgensen AO, Shen AC, Arnold W, Leung AT, Campbell KP. Subcellular distribution of the 1,4-dihydropyridine receptor in rabbit skeletal muscle in situ: an immunofluorescence and immunocolloidal gold-labeling study. *J Cell Biol* 1989; **109**: 135–147.
26 Kifor O, Diaz R, Butters R, Kifor I, Brown EM. The calcium-sensing receptor is localized in caveolin-rich plasma membrane domains of bovine parathyroid cells. *J Biol Chem* 1998; **273**: 21708–21713.
27 Isshiki M, Ando J, Yamamoto K, Fujita T, Ying Y, Anderson RG. Sites of Ca(2+) wave initiation move with caveolae to the trailing edge of migrating cells. *J Cell Sci* 2002; **115**(Pt 3): 475–484.
28 Isshiki M, Anderson RG. Function of caveolae in Ca2+ entry and Ca2+-dependent signal transduction. *Traffic (Copenhagen, Denmark)* 2003; **4**: 717–723.
29 Wieckowski MR, Giorgi C, Lebiedzinska M, Duszynski J, Pinton P. Isolation of mitochondria-associated membranes and mitochondria from animal tissues and cells. *Nat Protoc* 2009; **4**: 1582–1590.
30 Giorgi C, De Stefani D, Bononi A, Rizzuto R, Pinton P. Structural and functional link between the mitochondrial network and the endoplasmic reticulum. *Int J Biochem Cell Biol* 2009; **41**: 1817–1827.
31 Patergnani S, Suski JM, Agnoletto C, Bononi A, Bonora M, De Marchi E *et al.* Calcium signaling around mitochondria associated membranes (MAMs) *Cell Commun Signal* 2011; **9**: 19.
32 Pinton P, Rimessi A, Romagnoli A, Prandini A, Rizzuto R. Biosensors for the detection of calcium and pH. *Methods Cell Biol* 2007; **80**: 297–325.
33 Pantoja C, Serrano M. Murine fibroblasts lacking p21 undergo senescence and are resistant to transformation by oncogenic Ras. *Oncogene* 1999; **18**: 4974–4982.
34 Gallimore PH, Grand RJ, Byrd PJ. Transformation of human embryo retinoblasts with simian virus 40, adenovirus and ras oncogenes. *Anticancer Res* 1986; **6**(3 Pt B): 499–508.
35 Ferdek PE, Gerasimenko JV, Peng S, Tepikin AV, Petersen OH, Gerasimenko OV. A novel role for Bcl-2 in regulation of cellular calcium extrusion. *Curr Biol* 2012; **22**: 1241–1246.
36 Krejci P, Prochazkova J, Smutny J, Chlebova K, Lin P, Aklian A *et al.* FGFR3 signaling induces a reversible senescence phenotype in chondrocytes similar to oncogene-induced premature senescence. *Bone* 2010; **47**: 102–110.
37 Koleske AJ, Baltimore D, Lisanti MP. Reduction of caveolin and caveolae in oncogenically transformed cells. *Proc Natl Acad Sci USA* 1995; **92**: 1381–1385.
38 Hayer A, Stoeber M, Ritz D, Engel S, Meyer HH, Helenius A. Caveolin-1 is ubiquitinated and targeted to intralumenal vesicles in endolysosomes for degradation. *J Cell Biol* 2010; **191**: 615–629.
39 Pozzan T, Rizzuto R, Volpe P, Meldolesi J. Molecular and cellular physiology of intracellular calcium stores. *Physiol Rev* 1994; **74**: 595–636.
40 Lee SW, Reimer CL, Oh P, Campbell DB, Schnitzer JE. Tumor cell growth inhibition by caveolin re-expression in human breast cancer cells. *Oncogene* 1998; **16**: 1391–1397.
41 Racine C, Belanger M, Hirabayashi H, Boucher M, Chakir J, Couet J. Reduction of caveolin 1 gene expression in lung carcinoma cell lines. *Biochem Biophys Res Commun* 1999; **255**: 580–586.
42 Bender F, Montoya M, Monardes V, Leyton L, Quest AF. Caveolae and caveolae-like membrane domains in cellular signaling and disease: identification of downstream targets for the tumor suppressor protein caveolin-1. *Biol Res* 2002; **35**: 151–167.
43 Wiechen K, Diatchenko L, Agoulnik A, Scharff KM, Schober H, Arlt K *et al.* Caveolin-1 is down-regulated in human ovarian carcinoma and acts as a candidate tumor suppressor gene. *Am J Pathol* 2001; **159**: 1635–1643.
44 Wiechen K, Sers C, Agoulnik A, Arlt K, Dietel M, Schlag PM *et al.* Down-regulation of caveolin-1, a candidate tumor suppressor gene, in sarcomas. *Am J Pathol* 2001; **158**: 833–839.
45 Park DS, Razani B, Lasorella A, Schreiber-Agus N, Pestell RG, Iavarone A *et al.* Evidence that Myc isoforms transcriptionally repress caveolin-1 gene expression via an INR-dependent mechanism. *Biochemistry* 2001; **40**: 3354–3362.
46 Liu P, Rudick M, Anderson RG. Multiple functions of caveolin-1. *J Biol Chem* 2002; **277**: 41295–41298.
47 Rajjayabun PH, Garg S, Durkan GC, Charlton R, Robinson MC, Mellon JK. Caveolin-1 expression is associated with high-grade bladder cancer. *Urology* 2001; **58**: 811–814.
48 Galbiati F, Volonte D, Engelman JA, Watanabe G, Burk R, Pestell RG *et al.* Targeted downregulation of caveolin-1 is sufficient to drive cell transformation and hyperactivate the p42/44 MAP kinase cascade. *EMBO J* 1998; **17**: 6633–6648.
49 Volonte D, Zhang K, Lisanti MP, Galbiati F. Expression of caveolin-1 induces premature cellular senescence in primary cultures of murine fibroblasts. *Mol Biol Cell* 2002; **13**: 2502–2517.
50 Hulit J, Bash T, Fu M, Galbiati F, Albanese C, Sage DR *et al.* The cyclin D1 gene is transcriptionally repressed by caveolin-1. *J Biol Chem* 2000; **275**: 21203–21209.
51 Galbiati F, Volonte D, Liu J, Capozza F, Frank PG, Zhu L *et al.* Caveolin-1 expression negatively regulates cell cycle progression by inducing G(0)/G(1) arrest via a p53/p21(WAF1/Cip1)-dependent mechanism. *Mol Biol Cell* 2001; **12**: 2229–2244.

52 Song KS, Li S, Okamoto T, Quilliam LA, Sargiacomo M, Lisanti MP. Co-purification and direct interaction of Ras with caveolin, an integral membrane protein of caveolae microdomains. Detergent-free purification of caveolae microdomains. *J Biol Chem* 1996; **271**: 9690–9697.
53 Murata T, Lin MI, Stan RV, Bauer PM, Yu J, Sessa WC. Genetic evidence supporting caveolae microdomain regulation of calcium entry in endothelial cells. *J Biol Chem* 2007; **282**: 16631–16643.
54 Adebiyi A, Narayanan D, Jaggar JH. Caveolin-1 assembles type 1 inositol 1,4,5-trisphosphate receptors and canonical transient receptor potential 3 channels into a functional signaling complex in arterial smooth muscle cells. *J Biol Chem* 2011; **286**: 4341–4348.
55 Rimessi A, Giorgi C, Pinton P, Rizzuto R. The versatility of mitochondrial calcium signals: from stimulation of cell metabolism to induction of cell death. *Biochimica et biophysica acta* 2008; **777**: 808–816.
56 Berridge MV, Tan AS. Effects of mitochondrial gene deletion on tumorigenicity of metastatic melanoma: reassessing the Warburg effect. *Rejuvenation Res* 2010; **13**: 139–141.
57 Pavlides S, Tsirigos A, Vera I, Flomenberg N, Frank PG, Casimiro MC *et al*. Transcriptional evidence for the "Reverse Warburg Effect" in human breast cancer tumor stroma and metastasis: similarities with oxidative stress, inflammation, Alzheimer's disease, and "Neuron-Glia Metabolic Coupling". *Aging* 2010; **2**: 185–199.
58 Martinez-Outschoorn UE, Balliet RM, Rivadeneira DB, Chiavarina B, Pavlides S, Wang C *et al*. Oxidative stress in cancer associated fibroblasts drives tumor-stroma co-evolution: A new paradigm for understanding tumor metabolism, the field effect and genomic instability in cancer cells. *Cell cycle (Georgetown, Tex)* 2010; **9**: 3256–3276.
59 Guo JY, Chen HY, Mathew R, Fan J, Strohecker AM, Karsli-Uzunbas G *et al*. Activated Ras requires autophagy to maintain oxidative metabolism and tumorigenesis. *Genes Dev* 2011; **25**: 460–470.
60 Sano R, Annunziata I, Patterson A, Moshiach S, Gomero E, Opferman J *et al*. GM1-ganglioside accumulation at the mitochondria-associated ER membranes links ER stress to Ca(2+)-dependent mitochondrial apoptosis. *Mol Cell* 2009; **36**: 500–511.

Supplementary Information accompanies this paper on the Oncogene website (http://www.nature.com/onc)